Vis–NIR Reflectance Microspectroscopy of IDPs

Romain Maupin, Zahia Djouadi, Rosario Brunetto, Cateline Lantz, Alice Aléon-Toppani, Pierre Vernazza

The Planetary Science Journal, 1:62 (11pp), 2020 December https://doi.org/10.3847/PSJ/abbb98

Vis–NIR Reflectance Microspectroscopy of IDPs

Romain Maupin[1], Zahia Djouadi[1], Rosario Brunetto[1], Cateline Lantz[1], Alice Aléon-Toppani[1], and Pierre Vernazza[2]
[1] Université Paris-Saclay CNRS, Institut d'Astrophysique Spatiale F-91405, Orsay, France; romain.maupin@universite-paris-saclay.fr
[2] Aix Marseille Université CNRS, CNES, Laboratoire d'Astrophysique de Marseille, Marseille, France
Received 2020 June 17; revised 2020 September 22; accepted 2020 September 23; published 2020 November 9

Abstract

Visible near-infrared (Vis–NIR) reflectance spectroscopy is a powerful nondestructive technique allowing the parent bodies identification of cosmomaterials such as meteorites, micrometeorites, and interplanetary dust particles (IDPs) studied in the laboratory. Previous studies showed that meteorites do not represent the full diversity of the solar system small bodies. We present here an experimental setup we developed for measuring Vis–NIR microspectroscopy of individual IDPs. We acquired diffuse Vis–NIR reflectance spectra of 15 particles ranging 7–31 μm in size. We discuss the requirements, the abilities, as well as the limitations of the technique. For sizes smaller than 17 μm, the slopes increase with decreasing particles sizes, while for sizes larger than 17 μm, the slopes are randomly distributed. The visible reflectance levels do not appear to be affected by the size of the IDPs, and show a bimodal distribution. Among the studied particles, we identified an IDP (L2079C18) exhibiting a feature at 0.66 μm, which is similar to the one observed by remote sensing on the surface of hydrated asteroids. This is the first detection of a hydration band in the reflectance spectrum of an IDP that could indicate a possible link between hydrated IDPs with hydrated asteroid surfaces.

Unified Astronomy Thesaurus concepts: Spectroscopy (1558); Experimental techniques (2078); Interplanetary dust (821); Meteorites (1038); Asteroids (72); Comets (280)

1. Introduction

Asteroids and comets are the most primitive objects containing valuable clues about the physicochemical conditions of the early solar system. For decades, asteroids have been widely studied by spectroscopy to classify them (Tholen & Barucci 1989; Bus & Binzel 2002; DeMeo et al. 2009). Based on observations in the visible near-infrared (Vis–NIR) range (0.4–2.5 μm), the Bus-DeMeo taxonomy distinguishes 24 types, some of which included in a C-complex (B-, C-, Cb-, Cg-, Ch-, Cgh-types).

Meteorites have long been considered to be the best cosmomaterials representative of the surface of some asteroids. Vis–NIR reflectance measurements are often used to identify their parent bodies (e.g., McCord et al. 1970; Burbine & Binzel 2002 and references therein; Clark et al. 2011). However, meteorites are not representative of asteroids B-, C-, Cb-, and Cg-types, nor comets such as JFCs (Vernazza et al. 2015). Meteorite collections are affected by biases believed to be largely due to injection mechanisms into the inner solar system, mainly controlled by the Kirkwood gaps (Kirkwood 1891), and also due to atmospheric entry survival. Thus, identification of their parent bodies remains challenging.

Yet, for two decades, the sample return missions (Stardust, Hayabusa, Hayabusa2, and OSIRIS-REx) have enabled (and will allow for future samples) the analyses of well-identified asteroidal and cometary materials in the laboratory as well as in situ (e.g., Rosetta and Hayabusa2). Nevertheless, the quantity of returned sample is very limited and the analyses have to be managed very carefully.

Fortunately, we have access on Earth to a large amount of other extraterrestrial matter: about 40,000 tons of materials fall every year into Earth's atmosphere (Love & Brownlee 1993), mostly in the form of dust named interplanetary dust particles (IDPs). Since 1981, NASA has routinely collected IDPs in the stratosphere by using silicone oil-coated flat plate collectors deployed on the wings of high-altitude aircraft (Sandford 1987) and, more recently, collectors free of silicone (Messenger et al. 2015).

The chondritic IDPs have their elemental abundances approximating those of carbonaceous chondrites, conversely to nonchondritic ones (Rietmeijer 1998). We find chondritic porous IDPs (CP-IDPs) with a porosity as high as 70% and a mineralogy characterized by anhydrous silicates (pyroxene and/or olivine). The chondritic smooth IDPs (CS-IDPs) are characterized by a platy and/or fibrous surface textures and a mineralogy characterized by hydrated silicates (Bradley 2003). IDPs are very heterogeneous in composition at submicrometric scales, as they mainly consist of a matrix material in which particles of different compositions and different sizes are dispersed (e.g., Bradley 2003; Brunetto et al. 2011). Silicates are the major mineral component, giving three groups: olivine-rich IDPs (ol-rich), pyroxene-rich IDPs (px-rich), and layer-lattice silicate-rich ones (LLS-rich; Sandford & Bradley 1989). This silicate composition is often related to the particle structure, because generally CP-IDPs contain no or few hydrated silicates, which are instead the dominant component of CS-IDPs.

Unlike meteorites, dust orbits decay in spiral continuously toward the Sun by Poynting–Robertson drag (Brownlee 1994), allowing a wider sampling of solar system bodies. Several processes can produce cosmic dust such as small bodies collisions, impacts on the parent body surface with or without a weak atmosphere or the cometary activity (Rietmeijer 2002). Some main belt asteroids have episodic activity characterized by mass-loss events (Jewitt 2012), as well as some near-Earth asteroids as recently observed by OSIRIS-REx around the

B-type asteroid Bennu (Hergenrother et al. 2019; Lauretta et al. 2019).

The origin of cosmic dust is still widely debated. Based on the dynamics and/or study of zodiacal light a predominant cometary origin has been proposed (Liou et al. 1995; Hahn et al. 2002; Ipatov et al. 2008; Nesvorný et al. 2010; Yang & Ishiguro 2015 and references therein), while other authors proposed a predominant asteroidal origin (Dermott et al. 1984, 1996; Nesvorný et al. 2003; Tsumura et al. 2010). A possible link between some IDPs and comets has been experimentally established several times by measuring the He release patterns (Brownlee et al. 1995) or with IR measurements (Sandford & Walker 1985; Campins & Ryan 1989; Sandford & Bradley 1989; Wooden 2002, 2008; Brunetto et al. 2011; Schulz et al. 2015).

The link between IDPs and asteroids can be investigated thanks to Vis–NIR spectroscopy commonly used for the classification of asteroids. Reflectance measurements performed on individual micrometric particles remain poorly explored. A few studies reported reflectance measurements on IDPs in the range 0.4–0.8 μm (Bradley 1994; Bradley et al. 1996; Thomas et al. 1995). A possible link between hydrous IDPs and C-complex asteroids and between CP-IDPs with P- and D-type asteroids is mentioned (Bradley et al. 1996).

In 2015, Vernazza et al. simulated the reflectance spectra of surfaces with analog composition of IDPs in the Vis–NIR range (0.4–2.5 μm). They also compared IR spectra performed on IDPs (Merouane et al. 2014) with those of comets and asteroids B-, C-, Cb-, and Cg-types, not sampled by meteorites. They found a possible link between IDPs and these types of asteroids (Vernazza et al. 2015).

The Vis–NIR reflectance measurements constitute a powerful tool for identifying the parent body of the extraterrestrial material analyzed in the laboratory. However the results of the measurements acquired on small particles in the laboratory could be different from those performed by remote sensing on the whole surface of the solar system small bodies and those performed on meteorites in laboratory, prepared as a macroscopic surface (made up of a large quantity of particles). We must understand how the measurement on an isolated micrometric particle can be affected by the physical parameters of the sample: such as size, composition, roughness, etc. For macroscopic surfaces, there are multiple effects which come into play and which are studied experimentally and numerically (e.g., Mustard & Hays 1997; Craig et al. 2007; Hapke 2008 and references therein; Verpoorter et al. 2014). Unfortunately, for small isolated particles, the different parameters that can affect the reflectance measurement have not been explored.

We present here a device we implemented for reflectance measurements in the Vis–NIR (0.45–1.0 μm) range. We also report the results we obtained on 15 IDPs analyzed with our new setup.

2. Materials and Methods

2.1. Samples

We studied 15 IDPs provided by the JSC, NASA. These particles are from the collectors L2071, L2076, L2079, L2083, and W7068. One of them is classified as Cosmic (L2083G23) by the JSC, the other ones are classified as Possibly Cosmic. Table 1 summarizes the characteristics of the studied particles.

Table 1
Characteristics of the Studied IDPs

Particle	Size (μm)	Allocated Number	Reflectance Level (%)	Vis–NIR Slope (μm^{-1})
L2079C18	35 × 27	1	6.1 ± 0.5	−0.24 ± 0.01
L2079E29	37 × 22	2	6.1 ± 0.8	0.35 ± 0.01
W7068C40	25 × 23	3	6.5 ± 1.1	0.53 ± 0.01
W7068B18	22 × 20	4	3.3 ± 0.6	0.02 ± 0.01
L2071E34	22 × 20	5	2.7 ± 0.3	−0.28 ± 0.01
W7068C2	21 × 20	6	3.2 ± 0.4	0.38 ± 0.02
W7068B20	14 × 14	7_a	8.4 ± 1.3	1.13 ± 0.02
W7068B20	14 × 10	7_b	4.3 ± 0.7	1.64 ± 0.03
L2076C29	23 × 15	8	11.7 ± 0.6	0.43 ± 0.03
L2079D12	18 × 15	9	4.2 ± 0.7	0.33 ± 0.01
W7068C45	16 × 15	10	4.2 ± 1.0	0.34 ± 0.01
L2071E43	15 × 15	11	5.8 ± 0.4	0.94 ± 0.02
L2083E38	15 × 13	12	3.2 ± 0.7	1.24 ± 0.02
L2083G23*	11 × 11	13	2.6 ± 0.7	1.47 ± 0.03
W7068B37	9 × 9	14	2.9 ± 0.6	2.17 ± 0.02
L2083E39	8 × 6	15	1.2 ± 0.5	2.66 ± 0.03

Note. Characteristics of the studied IDPs classified by decreasing size, with 1 being the largest and 15 the smallest. The IDP W7068B20 (7) is broken into fragments 7_a and 7_b, the initial size was 23 μm × 18 μm. * indicates Cosmic particle. The reflectance level is extracted at 0.55 μm, and the Vis–NIR slope is calculated on the whole wavelength range.

We associate each particle to a number according to their decreasing size.

In addition to these particles, we used minerals and some meteorites as standards to perform preliminary measurements. Anhydrous silicates being the main constituent of CP-IDPs we chose forsterite and enstatite as minerals, which have absorption bands in the experimental range (0.45–1.0 μm). The characteristic absorption feature of forsterite is around 1 μm and is composed of three bands (e.g., Burns 1993), while enstatite has a single band around 0.9 μm (e.g., Cloutis & Gaffey 1991). These absorption bands are detected in some meteorites (e.g., Gaffey 1976; Cloutis et al. 1986) and on some asteroids (e.g., Gaffey et al. 1993; Sunshine et al. 1997; Burbine et al. 2003).

We also used the powder of four meteorites of different classes (Dar al Gani 684 (DAG 684), Gilgoin, Frontier Mountain 95002 (FRO 95002), and Allende), to investigate several reflectance levels (dark and bright), different features, and composition heterogeneity.

DAG 684 is an Eucrite from the Howardite–Eucrite–Diogenite family related to the Vesta asteroid (McCord et al. 1970). Eucrites are differentiated meteorites with a mineralogy dominated by plagioclase and pyroxene (Duke & Silver 1967). Eucrite reflectance spectra exhibit a broad feature of silicate around 0.9 μm (e.g., McCord et al. 1970; Gaffey 1976; Burbine et al. 2001; Beck et al. 2012).

Gilgoin is an ordinary chondrite H5 (Urey & Craig 1953). Ordinary chondrites have a mineralogy composition dominated by a mix of olivine and pyroxene with a varying amount of metallic Fe (Sears & Dodd 1988). Reflectance spectra of ordinary chondrites show an absorption band around 0.9 μm.

FRO 95002 is a carbonaceous chondrite (CO3). CO meteorites contain a large fraction of porphyritic olivine-rich chondrules (35–45 *vol.%*) with a small size (∼150 μm; Rubin 1989). The majority of CO meteorites have a matrix dominated by olivine (Brearley & Jones 1998), and some of

CO meteorites show signs of aqueous alteration of matrix (Keller & Buseck 1990; Brearley 1993). Reflectance spectra of this meteorite show a slight silicate absorption band in the experimental range.

Allende is a carbonaceous chondrite (CV3). CV meteorites are characterized by a large fraction of mm-sized porphyritic olivine and pyroxene-rich chondrules. The matrix mineralogy is dominated by olivine (Brearley & Jones 1998), and some of them are characterized by the presence of phyllosilicates (saponite and serpentine), signs of aqueous alteration (e.g., Keller & Buseck 1990; Tomeoka & Buseck 1990; Bonal et al. 2006). Reflectance spectra of this meteorite are characterized by a low reflectance level and show a slight silicate absorption band.

The sample powder (without sorting the particle size) was deposited in a sample holder and a flat surface is obtained by removing the excess of materials. This sample preparation is similar to what is currently used for other meteorite reflectance measurements.

2.2. Experimental Setup

Our setup, installed in a clean room, consists of a Vis–NIR (0.3–1.1 μm) grating spectrometer Maya2000 Pro (Ocean Optics) with 4.5 nm spectral resolution coupled to a macroscope (Leica Z16 APO), inspired by the setup of Bonal et al. (2015). The sample holder is placed on a rotative platform, allowing rotations in the horizontal plane and its vertical position is set to adjust the focus. A Vis–NIR optical fiber (50 or 100 μm in diameter) is positioned orthogonally to the sample to collect the light diffused by the sample (at 0°). The sample is unilaterally illuminated (at 45°) by a 1000 μm diameter fiber which is coupled to a Halogen source. Due to the optics of the macroscope the accessible spectral range is reduced to 0.45–1.0 μm. By changing the magnification and/or the diameter of the collection fiber it is possible to adjust the collection spot to the particle size down to 7 μm, without using any diaphragm.

We performed measurements at millimetric scales (collection spot $\sim$ mm) and measurements at micrometric scales (collection spot $\sim$ μm). In this last case, the use of the macroscope is necessary to adjust the collection spot to the size of the isolated particles. In the case of millimetric measurements, the powder samples (meteorites) are unilaterally illuminated at 45° with a 1000 μm diameter optical fiber and the reflected light by the sample is collected at 0° by an optical fiber of 100 μm in diameter. In this case, the collection spot size is about 3 mm, large enough to take into account the whole heterogeneity of the samples, which is not the case with a micrometric collection spot. Another difference between millimetric and micrometric measurements is the distance between the illumination fiber and the sample, $\sim$5 cm and $\sim$1 mm, respectively. This latter distance is small enough to make the measurements sensitive to the sample surface irregularities.

In both cases (measurements at millimetric and micrometric scales), reference spectra were collected with respect to a 99% Spectralon standard (from Labsphere).

3. Results

3.1. Preliminary Measurements

We first performed millimetric and micrometric measurements on minerals and meteorites to verify the possibility to retrieve the characteristic features of the sample with a 12 μm spot size (intermediate spot size used in this study). With a micrometric spot size, the collection spot can be smaller than the heterogeneity scale of the sample surface. The obtained reflectance spectrum depends on the position of the micrometric collection spot on the surface of the sample. It is thus necessary to average different spectra taken at different locations in the studied sample to get its overall signature. Because the distance illumination fiber sample is smaller in the case of the micrometric measurements than in the millimetric ones, a direct comparison between the obtained reflectance spectra, in terms of reflectance level, is not easy, thus we normalized each spectrum at 0.55 μm.

Figure 1 compares normalized spectra obtained with a collection spot of 3 mm (gray) and the average of 100 spectra obtained at different random positions with a collection spot of 12 μm (black) for each sample used as standards in this study. This figure clearly illustrates in each case a good agreement between the two spectra. It thus validates the procedure of averaging different microscopic contributions to retrieve the signatures obtained with a millimeter spot.

Once we validated the measurement at microscopic scales, we investigated the effect of the orientation of an isolated particle with respect to the illuminating light (azimuthal angle, φ, varying between 0° and 360°). To do so, we acquired spectra on a particle ($\sim$30 $\times$ 30 μm) of DAG 684 meteorite with different orientations with respect to the incident light (by varying the φ angle). The reflectance spectra obtained by averaging 4, 8, 20, and 40 orientations are shown in Figure 2(a). A convergence between 20 and 40 rotations is observed. We must therefore consider 20 successive rotations of 18° each (ensuring an illumination of the particle at 360°), and average the obtained spectra to obtain the reflectance spectrum of an isolated particle. As the DAG 684 meteorite is heterogeneous in composition at the scale of the particle (micrometric scale), it is impossible to reproduce its global spectrum (obtained with millimetric collection spot) by using a single micrometer particle. However, comparing Figures 1(c) and 2(a) one can see that the silicates band $\sim$0.940 μm is obtained in both cases, although the overall spectral shape is different, including the dissimilar position of the reflectance maximum.

To evaluate the dispersion in reflectance of a spectrum at a φ angle value (spectrum φ) from the average (as illustrated for DAG in Figure 2(b)), we introduced the following variable:

$$\Delta_{\varphi}(\%) = \frac{\sum_{\lambda} |r_{\varphi,\lambda} - R_{\lambda}|}{N}, \quad (1)$$

with $r_{\varphi,\lambda}$ as the reflectance of the spectrum at φ angle value at the wavelength λ; R_{λ} as the reflectance of the average spectrum at the wavelength λ; and N as the spectral points. This quantity is averaged over the entire spectral range and therefore includes changes in reflectance, but it does not account for shape variation. To evaluate only the change in the shape of the spectrum φ from the average, we calculate the same quantity but with normalized spectra at 0.55 μm after dividing each φ spectrum by the average spectrum:

$$\Delta_{\varphi}^{\mathrm{norm}} = \frac{\sum_{\lambda} \left| \frac{r_{\varphi,\lambda}^{\mathrm{norm}}}{R_{\lambda}^{\mathrm{norm}}} - 1 \right|}{N}, \quad (2)$$

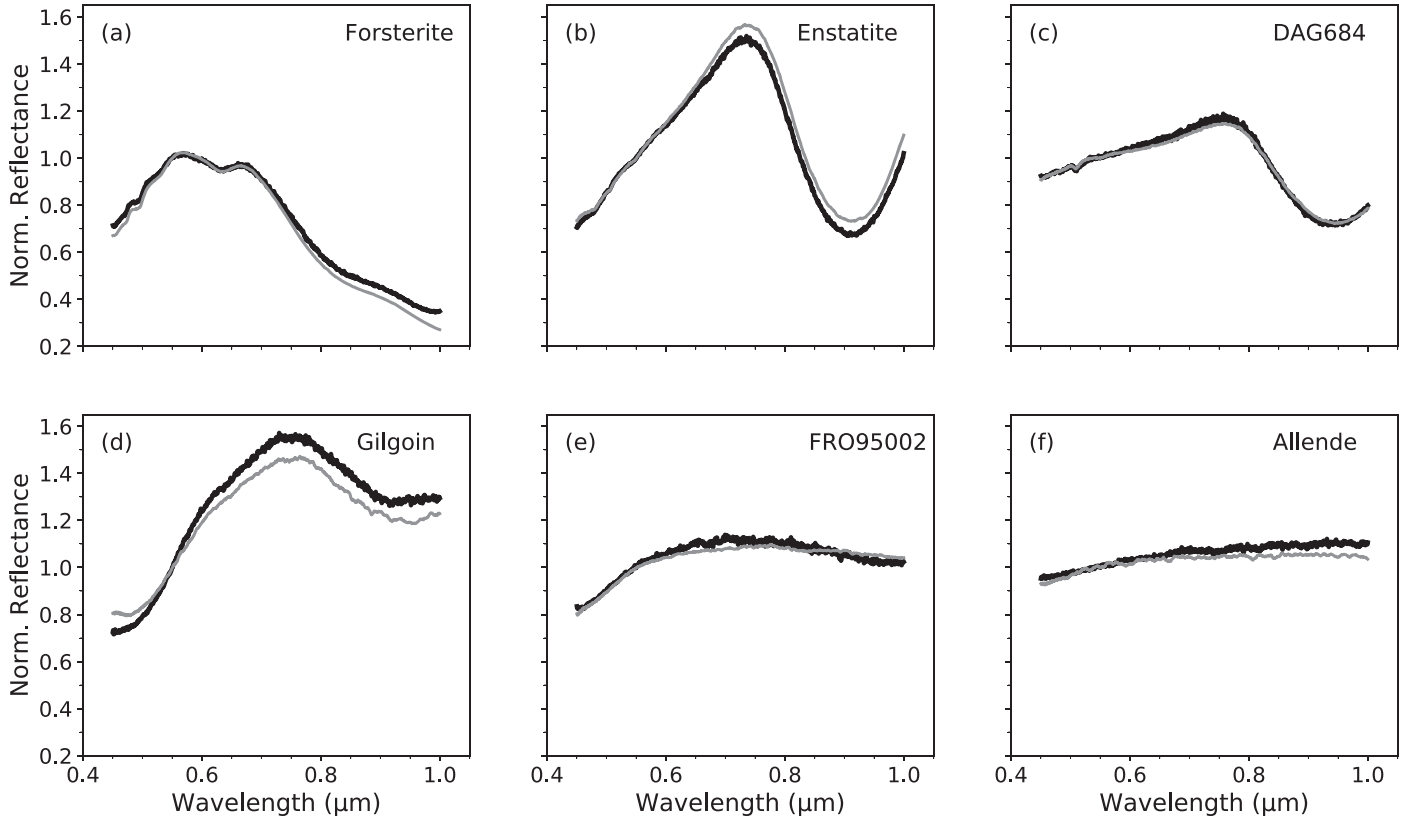

Figure 1. Comparison between the millimetric measurements on powders (collection spot ~3 mm) in gray and the average of 100 micrometric measurements on isolated particles (collection spot 12 μm) in black, on different minerals and meteorites (Dar al Gani 684 (DAG 684), Gilgoin, Frontier Mountain 95002 (FRO 95002), and Allende) used as standards in this study.

with $r_{\varphi,\lambda}^{\mathrm{norm}}$ as the reflectance of the normalized spectrum φ at the wavelength λ, and $R_{\lambda}^{\mathrm{norm}}$ as the reflectance of the normalized average spectrum at wavelength λ. For the DAG particle, we found $\Delta = 3.9 \pm 0.5\%$ and $\Delta^{\mathrm{norm}} = 0.0462 \pm 0.0003$ (averaged over the 20 φ values). Thus, for this particle, the reflectance dispersion is important, but the spectra at different φ values have a shape close to the shape of the average spectrum.

In the following, the "spectrum of the particle" designates the spectrum obtained by averaging the 20 φ spectra.

3.2. Uncertainties Estimation

Various sources of uncertainties in the micromeasurements can affect the reflectance level and/or the slope of the spectrum. We describe in this section the uncertainties sources and their estimation.

3.2.1. Reflectance Level Uncertainty

As mentioned, the reflectance of the sample is determined relative to a spectralon reference. The reflectance levels can be affected by different parameters.

(i) When observed under a macroscope, the spectralon exhibits topographical variations higher than the collection spot size. The reference spectra can thus vary according to the position where they are acquired. To evaluate this effect, for each collection spot size (7, 12, and 16 μm) we acquired 100 spectra at different positions on the spectralon and averaged them. Each spectrum is thus divided by the average to deduce the reflectance in each position; the reflectance has to be about 100% if each position gave the same reflectance. The dispersion of reflectance is then determined to estimate the uncertainty, due to the random positions of the spot on the surface of the spectralon during the measurements. We found a value of $\delta R_{\mathrm{ref}} \sim 0.5\%$ (evaluated at 1σ) over the entire wavelength range and for all spot sizes, which is low compared with the reflectance levels of most IDPs (see Section 4.3).

(ii) The second effect is due to the focus, a difference in vertical position between the particle and the spectralon can affect the reflectance level.

As these effects cannot be easily managed and to improve the signal-to-noise ratio (S/N), we performed a series of three measurements having different starting azimuth angle (0°, 6° and 12°). Changing the starting azimuthal angle allows to sample more orientations than for a single measurement. These three measurements are then averaged, and an uncertainty is deduced by taking the dispersion around the average of the three measurements (σ). To encompass the weak sampling of measurement, we applied to the incertitude a student factor of $t \sim 4.3$. Finally, the reflectance uncertainty is deduced by using the formula:

$$\delta R = \sqrt{t \times \sigma + \delta R_{\mathrm{ref}}}. \quad (3)$$

3.2.2. Slope Uncertainty

The slope of a spectrum is calculated by a linear fit of the spectrum over a given interval (DeMeo et al. 2009). Depending on the point chosen on the spectralon as reference for the measurement, the slope of the reflectance spectrum may vary. To evaluate the dispersion of the slope due to the spectralon on

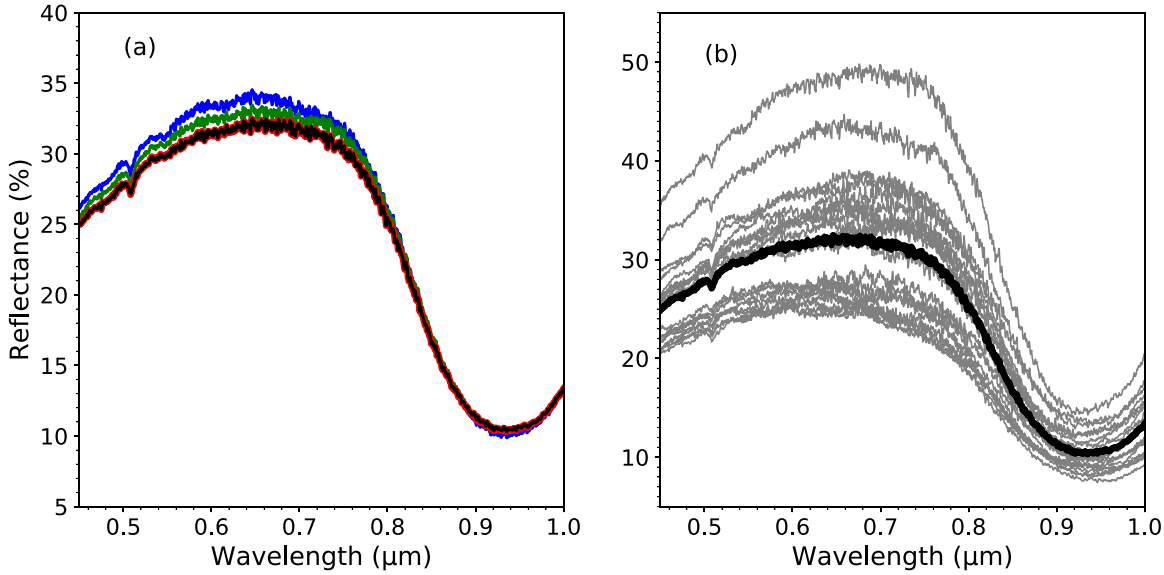

Figure 2. (a) Reflectance spectra obtained on an isolated particle (~30 μm) from DAG 684 with 4 (blue), 8 (green), 20 (red), and 40 (black) rotations. (b) Comparison between the average with 20 rotations (black) and the 20 individual spectra (gray).

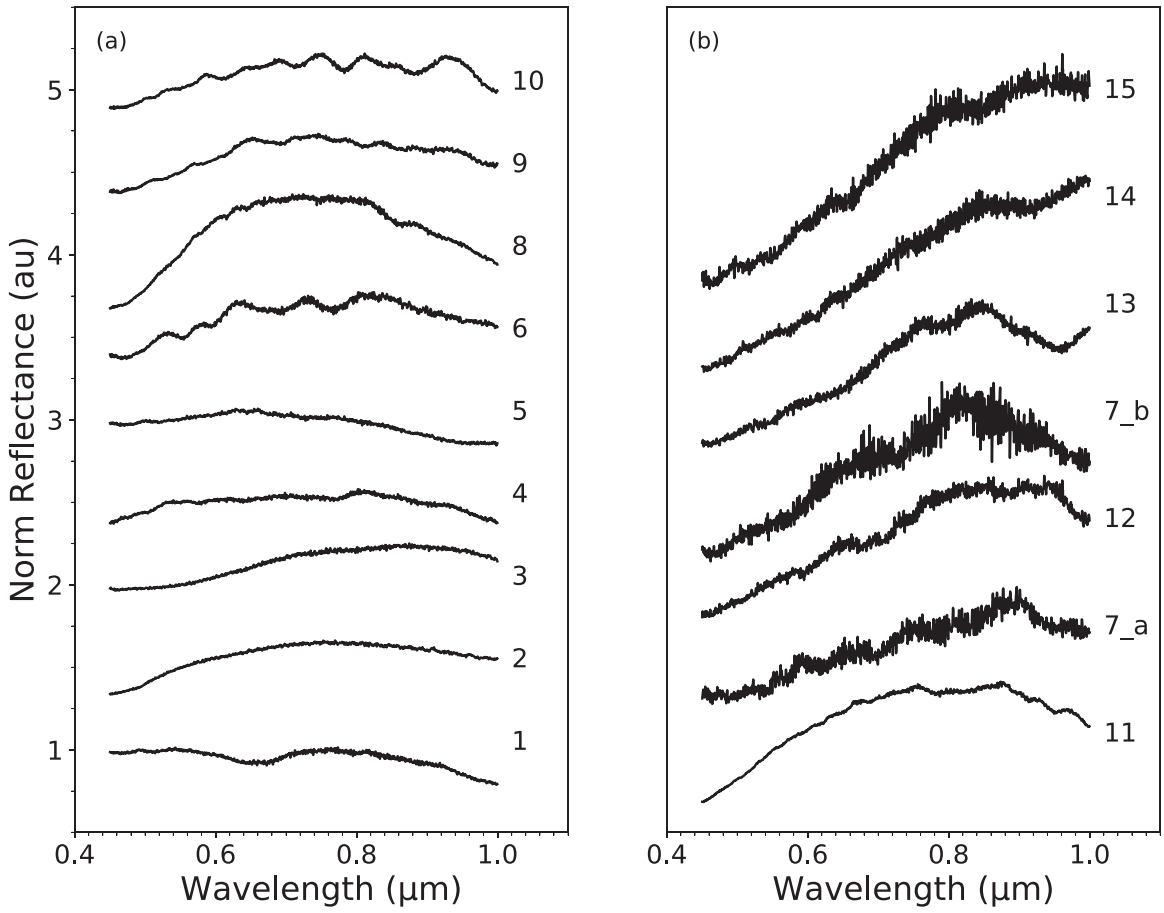

Figure 3. Reflectance spectra normalized at 0.55 μm of the 15 IDPs, sorted by particle size and vertically shifted for clarity. Spectra 7 and 12 to 15 are obtained with a 50 μm fiber, the others are obtained with 100 μm fiber.

the entire range (0.45–1.0 μm), we use the 100 spectra used to evaluate the dispersion in reflectance (see Section 3.2.1). We found an uncertainty on the slope (for different spot sizes) of the order of ~0.005 μm^{-1}. This uncertainty is evaluated at 1σ.

3.3. Reflectance Spectra of IDPs

We first acquired reflectance spectra of the glass slide (samples holders) as well as the silicon oil (as a precaution, although IDPs are free of silicone oil) to check whether they have specific signatures in the considered range. We found that

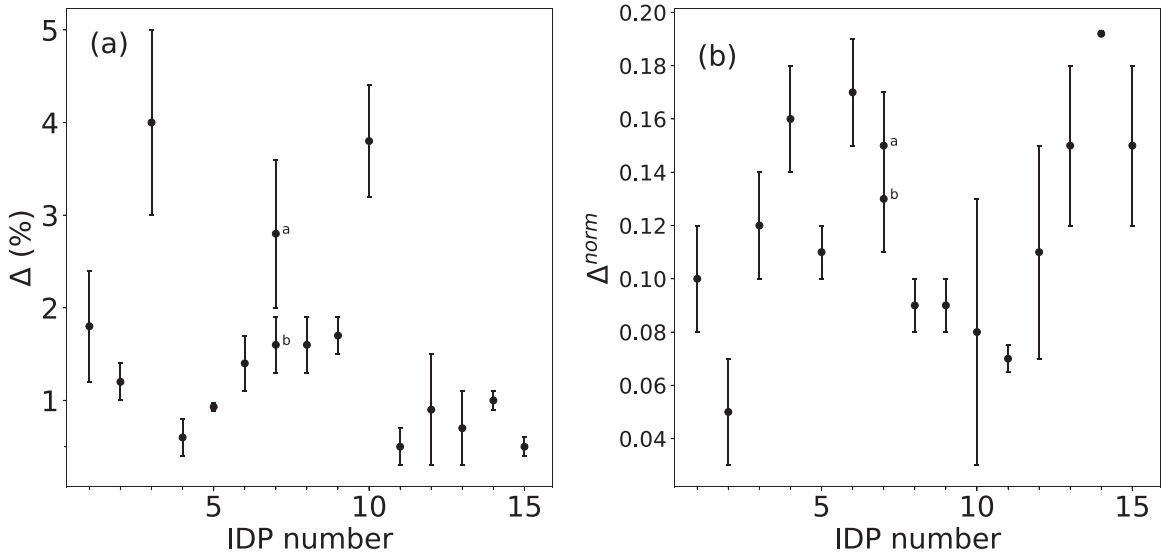

Figure 4. (a) Dispersion around the average spectrum (Equation (1)) and (b) dispersion around the average normalized spectrum (Equation (2)) for each IDP (numbers 1–15). The uncertainties are determined at 1σ between the three acquisitions (obtained by changing the initial azimuthal angle).

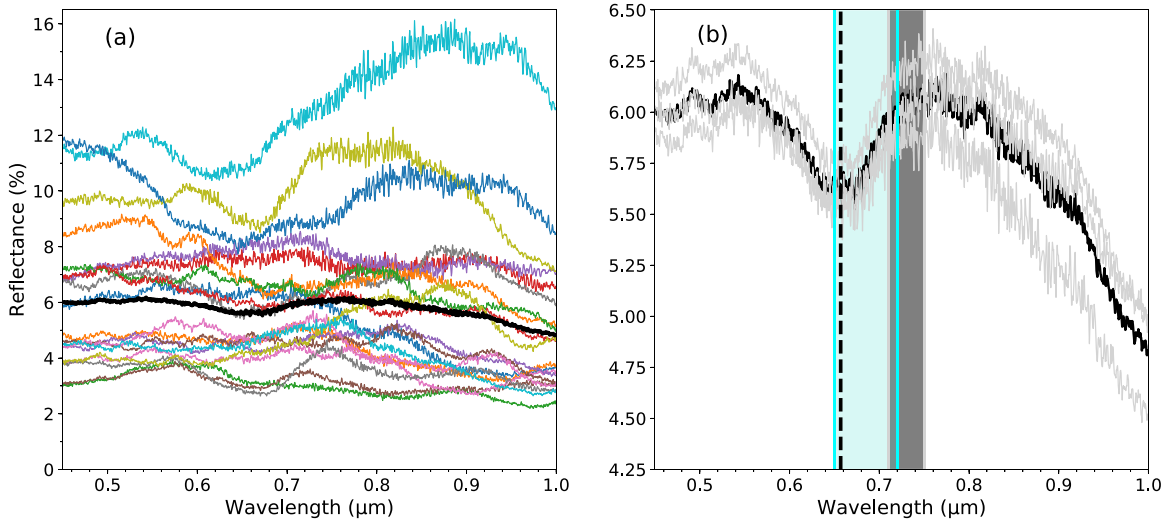

Figure 5. (a) Comparison between 20 individual spectra (colors) and the average (black) for the particle L2079C18 (1). (b) Comparison between the three spectra (gray) taken with different starting azimuthal angle and the average of this three spectra (black). The dotted line points out the absorption band at ∼0.66 μm. The light blue zone corresponds to the range of band positions for asteroids with a hydration band and the gray zone to the position of the bands of CM-type meteorites (Fornasier et al. 2014).

neither the glass slides nor the silicon oil has an effect on the result of the reflectance measurements because they have no diffuse reflectance (<0.1%), and no signatures in the wavelength range used here.

Figure 3 shows the set of reflectance spectra obtained on the 15 IDPs reported in Table 1. The spectra are normalized at 0.55 μm and shifted for clarity; they are more or less noisy depending on the collection fiber used, with the 100 μm diameter fiber having a better S/N than the 50 μm diameter fiber. Some spectra have many interference fringes (particles 6, 9, and 10). Note that spectrum 1 has a wide band at ∼0.66 μm, while the spectra 13 and 14 have a band close to 0.9 μm. For each particle, we calculated the reflectance levels before normalization at 0.55 μm (covering a wide range from ∼1 to 11% at 0.55 μm) and the spectral slope (from slightly blue ($-0.28\ \mu m^{-1}$) to red ($2.66\ \mu m^{-1}$)) over the entire wavelength range (see Table 1).

Figure 4 shows the dispersion, Δ (Figure 4(a)) and $\Delta^{\rm norm}$ (Figure 4(b))) calculated for the 15 IDPs (see Equations (1) and (2)). We note that the change in reflectance (Figure 4(a)) is not too large for IDPs, less than ∼2%, except for the particles 3, 7_a and 10. However, the dispersion in terms of shape of the different spectra (Figure 4(b)) is higher for all particles (except particle 2), indicating a strong variation in spectral shape for all φ spectra. As shown in Figure 5(a) in the case of the L2079C18 (1) particle with $\Delta^{\rm norm} \sim 0.10$. Particle L2079E29 (2) is the only particle with a weak value of shape dispersion with $\Delta^{\rm norm} \sim 0.05$ (of the same order of magnitude as for DAG particle), implying that all φ spectra are alike in terms of shape. Figure 5(b) shows (in light gray) the three spectra obtained by changing the starting azimuthal angle (see Section 3.2.1) and their average spectrum (in black). These three spectra exhibit a strong band around 0.66 μm, which will be discussed in Section 4.4.

4. Discussion

4.1. Measurements on Micrometric Particles

The measurements performed on mineral and on meteorite powders with millimetric and micrometic collection spots show that it is possible to obtain the same reflectance spectrum by averaging different microscopic contributions of the surface (see Figure 1). A millimetric collection spot comprises a large set of different orientations of the surface particles with respect to the incident light and can encompass all the heterogeneities (composition and surface structure), while the micrometric collection spot could be at the particle scale ($\sim \mu$m) and could therefore be below the scale of composition heterogeneity. This allows to take into account all the orientations and heterogeneities of composition and thus to recover the macroscopic signature.

The measurements on an isolated particle are different from the measurements on a whole surface (comprising a large number of particles). The illuminating light being unidirectional, in our setup, a spectrum taken at one orientation of the particle with respect to the illuminating light (i.e., one value of φ) is not representative of the whole particle. To obtain the spectrum of an isolated particle, it is therefore necessary to take into account its different orientations with respect to the incident light. The results obtained on a particle of the meteorite DAG, show that the reflectance spectrum converges, between 20 and 40 rotations (see Figure 2(a)). Figure 2(b) shows that in the case of the DAG particle, reflectance spectra at different φ values are close to the average spectrum in term of shape but not in term of the reflectance level. However the different φ spectra can be very different to the average spectrum as illustrated for the particle L2079C18 (1) in Figure 5. All IDPs (except particle 2) show large variations in their spectral shapes (Figure 4(b)). It is therefore necessary to measure at different azimuths to get the right level of reflectance and to be able to detect the absorption bands. This is the case of L2079C18 (1) whose average spectrum shows an absorption band at $\sim$0.66 μm which is difficult to identify on the spectra at different φ values (Figure 5(a)). The study of the φ spectra shows that the band is presented only on 9 spectrum on consecutive orientations (to orientation 6 at 12 and 18 at 19), indicating that the hydrated phase of the IDP is expressed only under some orientations and that it is therefore necessary to perform all the orientations to best constrain this characteristic.

4.2. Spectral Slope versus Particle Size

From Figure 3(b) and Table 1 one can notice that for the smallest particles the spectral slope tends to increase (reddening) with the decreasing size.

To evaluate this, we calculated the slope of the spectra in the Vis–NIR (0.45–1.0 μm) and introduced an "equivalent area" for each particle given by the product of its larger axis by its smaller one divided by π. We report in Figure 6 the Vis–NIR slope in the wavelength range versus the equivalent area (in μm^2).

From Figure 6 we can see two different trends. Larger particles (particles 1, 2, 3, 4, 5, 6, and 8) appear to have a slope that does not depend on the particle size (linear fit with $R^2 \sim 0.07$), with slopes distributed around 0 (-0.28 to 0.43 μm^{-1}), while for the smaller IDPs (particles 9, 10, 11, 12, 13, 14, 15, 7_a and 7_b) the slopes appear to be aligned along

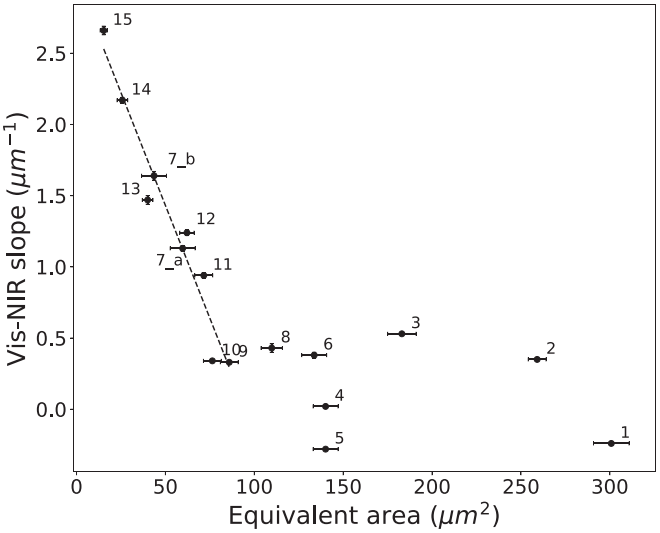

Figure 6. Spectral slope (calculated over the whole range) as a function of the equivalent surface area of the particles. The numbers are those of the particles (reported in Table 1).

a line showing a rapid increase in the slope when the size decreases. The best linear fit ($R^2 \sim 0.95$) is the one that connects particles 9–15. In this range of sizes, the slopes increase rapidly and become very red (distributed between 0.33 to 2.66 μm^{-1}). In the same way, particles having an equivalent area greater than particle 8 are more dispersed than small particles around the best linear fit of the distribution. The dispersion (D) is calculated as the average of the distance of the points to the best linear adjustment and we found $D = 0.33 \pm 0.06$ for particles with size factor greater than 100 μm^2 and $D = 0.04 \pm 0.01$ for the small ones.

This difference between small and large particles could be indicative of a physical bias in the measurement and/or a chemical bias due to alteration, such as atmospheric entry.

When we reduce the collection spot size to 7 μm (initially 10 μm) on the particle 12, we find a slope of 1.47 μm^{-1} (initially 1.24 μm^{-1}). We obtain an increase of the slope of 19% when the spot size is decreased by 30%, so in this wavelength range, and for small particles in addition to the influence of the particle size on the slope, it seems that the spot size also influences the slope of the spectrum. We interpreted this effect as a consequence of a physical and/or chemical bias. Reducing the spot is equivalent to considering a smaller particle of 30%, i.e., with an equivalent area from $\sim$62 to $\sim$43 μm^2, corresponding to the equivalent area of the particle 13 which has a slope of 1.47 μm^{-1} (see Table 1). However, this effect could also be due to a heterogeneity in composition, because the surface probed on the particle with the two collection spot sizes (7 and 10 μm) is no longer exactly the same and some IDPs may be mineralogically heterogeneous on a submicrometer scale (Bradley 2003).

We also assess whether this linear correlation between the particle size and the slope depends on the wavelength on which the slope is calculated. The slope is calculated over reduced ranges, [0.45–0.8] μm (Figure 7(a)) and [0.45–0.6] μm (Figure 7(b)).

For the first interval [0.45–0.8] μm (Figure 7(a)), a linear correlation still remains for the same particles (as in Figure 6), but the alignment is much worse than for the full interval ($R^2 \sim 0.78$) and the dispersion around the best linear fit also

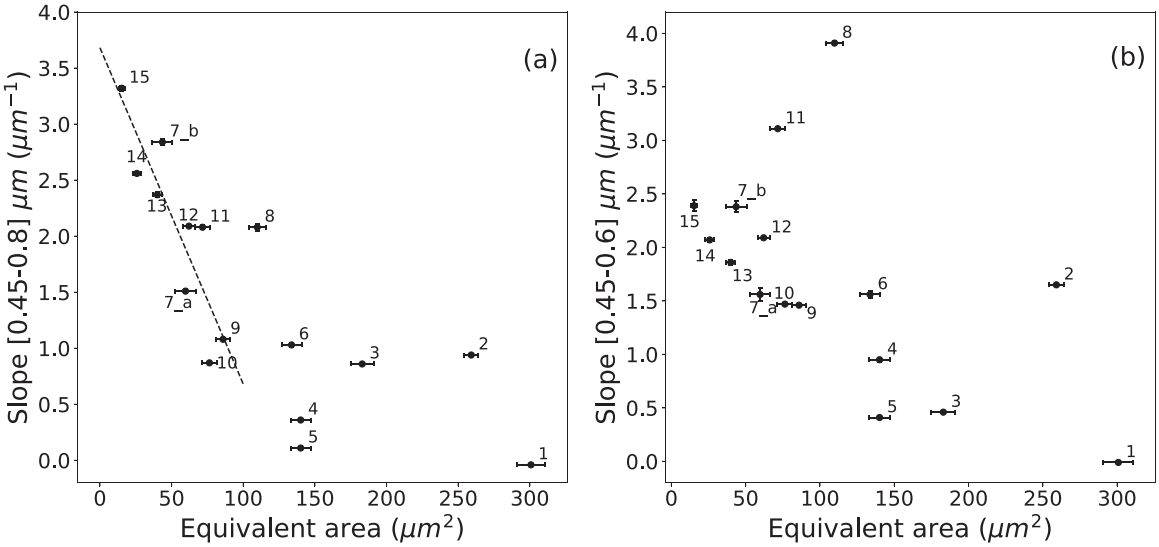

Figure 7. Spectral slope (calculated over [0.45–0.8] μm (a) and [0.45–0.6] μm (b)) as a function of the equivalent surface area of the particles.

increases ($D = 0.08 \pm 0.02$ versus 0.04 for the whole range). For the other particles it is still impossible to find a satisfactory linear adjustment. Note that in this wavelength range and for small particles, the spot size no longer seems to play a role because the slope obtained for the two spot sizes on the particle 12 are identical.

For the second interval [0.45–0.6] μm (Figure 7(b)), the linear correlation seems more difficult to establish. The best linear fit is weak ($R^2 = 0.09$) and the dispersion has increased significantly ($D = 0.20 \pm 0.06$). The two measurements on the particle 12 gave also the same result, so the spot size does not affect the slope. It is therefore a phenomenon dependent on the wavelength (what is expected for a physical and/or chemical bias); indeed, if one calculates the spectral slopes on smaller intervals (by considering the part of the short wavelengths of spectrum), the slope/size correlation is progressively lost.

For a wavelength interval there is a certain critical size below which the measurement is biased and the IDP spectrum cannot be used for comparison with a millimetric measurement. For the whole Vis–NIR range [0.45–1.0] μm used in this study, the critical size appears to be between the size of the IDPs 8 and 11 (between 71 and 110 μm^2). As a first approximation, we can define an average equivalent area around which the transition appears: $91 \pm 25\ \mu m^2$, which corresponds to an IDP with an equivalent diameter of: $17 \pm 2\ \mu$m. Thus, we can say that a measurement on an IDP in the Vis–NIR range [0.45–1.0] μm is not biased for IDPs with an equivalent diameter above 17 μm. For example, in the case of the DAG 684 meteorite, the spectra obtained on a whole macroscopic surface and on a big isolated particle ($\sim$30 μm) show the same absorption band. Bonal et al. (2015) performed reflectance measurements ([0.45–1.0] μm) on Itokawa particles of 30 and 54 μm, they found a good match between the spectra of the isolated particles with the asteroids spectrum. All of these corroborate the idea of a critical size of $17 \pm 2\ \mu$m to be able to analyze an IDP by Vis–NIR reflectance.

4.3. Reflectance Levels

In the discussion of the reflectance level at 0.55 μm, the smallest particle (number 15) is not considered. We show in Figure 8 the reflectance levels at 0.55 μm versus the equivalent area of the particles and no correlation with the particle size is observed. The absence of correlation between the reflectance level and the particle size is in good agreement with Hartman & Domingue (1998), who showed that the photometric properties of isolated particles remained unchanged at 0.55 μm for sizes down to 20 μm in diameter.

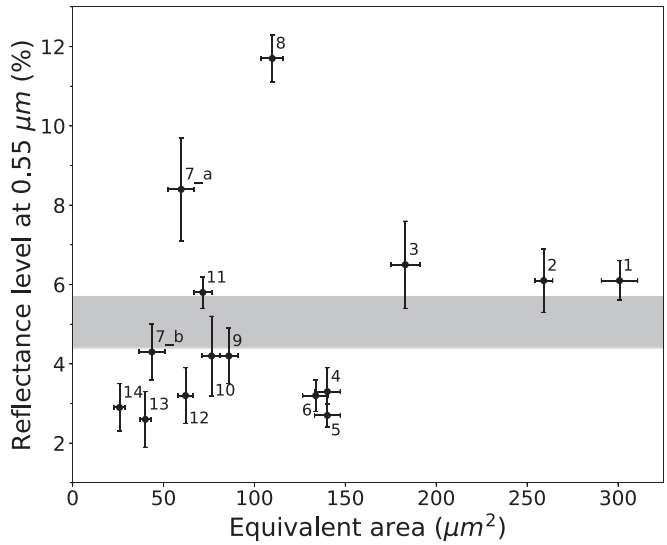

Figure 8. Reflectance level at 0.55 μm as a function of the equivalent area. Gray area points out the gap around 5% of reflectance.

The low reflectance levels found here for some IDPs ($\sim$2.6%) indicate that they could be analogous to very dark asteroids like Ryugu (C-type), whose reflectance at 0.55 μm is $1.88 \pm 0.17\%$ (Sugita et al. 2019; Watanabe et al. 2019). Note that the reflectance levels measured here are compatible with those measured on IDPs by Bradley et al. (1996) and on cometary particles with COSIMA (Langevin et al. 2020).

From Figure 8, if we except IDP 8, whose reflectance level is about 12%, one can define two groups, and a gap around a reflectance level of 5.05% is observed. The first group consists of the particles with a reflectance level higher than $\sim$5% (with an average of 6.6% and standard deviation of 1.0%) and the second group consists of the particles with a reflectance level

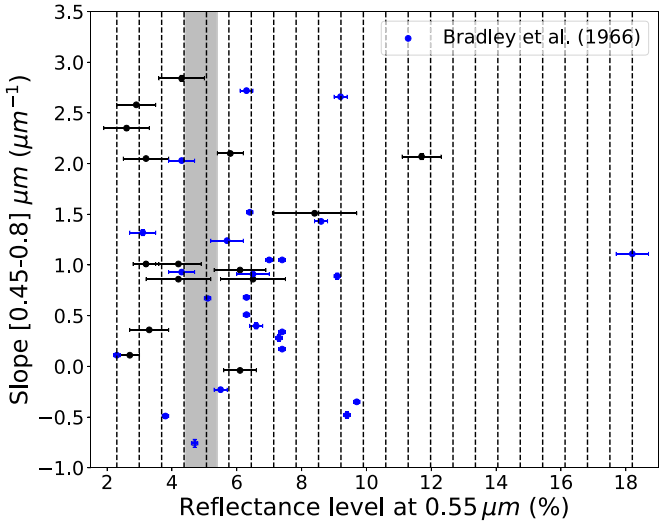

Figure 9. Spectral slope (0.45–0.8 μm) as a function of the reflectance level at 0.55 μm for our data set (black) and the Bradley et al. (1996) data set (blue points). The dotted lines represent the classes used to plot the histogram of the reflectance levels. Gray area points out the gap around 5% of reflectance.

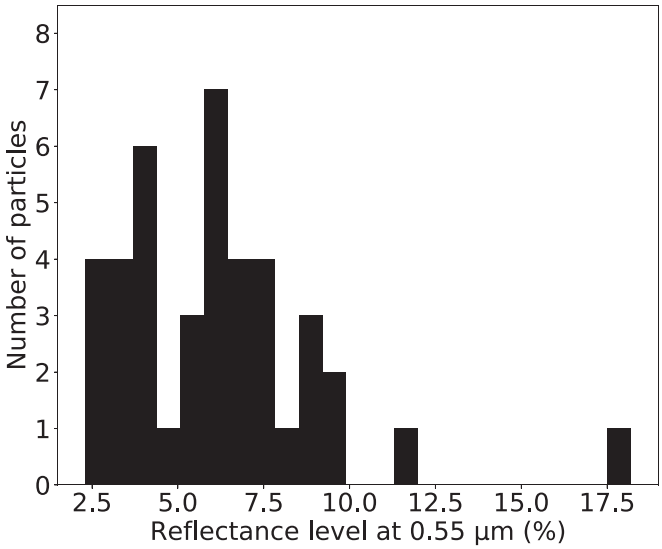

Figure 10. Histogram of the reflectance levels for the data set of the article and that of Bradley et al. (1996). The width of the classes is 0.8%.

less than ∼5% (with an average of 3.4% and standard deviation of 0.7%).

A T-test is performed to explore how the two groups are distributed relative to each other. We found $tobs \sim 6.13$, $p \sim 0.0009$ et $ddl = 12$, suggesting that the two groups are a priori distinct from each other despite the small sampling. Future reflectance measurements will complete the current sampling to obtain better statistics on the distribution of reflectance levels. Far IR, Raman analyzes on the IDPs are planned to study a possible link between this gap and the mineralogy of the IDPs.

To support the fact that this effect is not due to a single point in the spectrum (0.55 μm where the reflectance level is extracted), the same analysis was made by integrating part of the visible spectrum of each particle from 0.45 to 0.7 μm, and the same trend is obtained: two separate groups are found.

We also compare our data set with that of Bradley et al. (1996). Figure 9 shows the visible spectral slope (0.45–0.8 μm) as a function of the reflectance level at 0.55 μm for the two data sets. The two data sets are in good agreement because they cover a similar range. Certain points of the two data sets are grouped together, indicating that certain IDPs have very similar spectral parameters (slope and reflectance level).

In this same figure, we observe the same gap as before around 4.9%, most IDPs thus have a reflectance level which is either higher or lower than 5%. To highlight this characteristic, Figure 10 shows the histogram of the reflectance levels. The width of the classes was chosen to be equal to the average of the uncertainties on the reflectance levels (∼0.69%), as indicated in Figure 9 by the dotted lines. In this histogram, we distinguish three different distributions. A first with an average reflectance level of 3.4% (standard deviation of 0.6%), a second with an average reflectance level of 6.5% (standard deviation of 0.7%), and the third with an average reflectance level of 9.1% (0.4% standard deviation). With this new statistic, we find the first two groups identified previously in this study. There are also two IDPs that stand out from these three distributions with much higher reflectance levels than the others, ∼12% and ∼18%.

4.4. Absorption Bands

Figure 3 shows that interference fringes (periodic structures found in a spectrum) are present on many spectra. These interferences prevent the detection of potential absorption bands on these spectra but could also be indicative of a crystalline structure. For each particle of the *a* panel, we confirm the detection of an absorption band only if there are no interferences or if they are shallower and wider than the absorption band. For the panel b (smallest IDPs) because of a potential physical and/or chemical bias, bands must be interpreted with caution. For example, a band appears to be present for the smallest particles (13, 14, 15) in the silicate region ∼0.9 μm and the wavelength position of this band decreases with decreasing particle size (best linear fit with $R^2 \sim 0.98$). This linear displacement of the band complicates the interpretation that can be made. Indeed, these bands could be indicative of a silicate composition but their position and depth could be affected by the reddening of the continuum. Another possible interpretation could be that these bands are interferences appearing below a certain particle size in a red continuum.

L2079C18 (1) is the largest IDP analyzed here, it is therefore possible to exploit its whole spectrum. L2079C18 exhibits an absorption band around 0.66 μm (depth of 8.0 ± 0.6% relative to the continuum, much deeper than the possible interferences found in the spectrum with depth of ∼1.3%). The 0.66 μm band can be attributed to phyllosilicates that have signatures in the 0.6–0.75 μm region, due to Fe^{3+}–Fe^{2+} absorption. The position of the band depends on the composition and the type of phyllosilicate. Fe^{3+}–Fe^{2+} absorption appears mainly at wavelengths <0.7 μm for saponite, whereas serpentines mainly signs at wavelengths >0.7 μm (Cloutis et al. 2018). These two types of phyllosilicates are found in extraterrestrial matter in different proportions that may indicate different origins and/or histories. For example, CM chondrites have a mineralogy dominated by serpentines, CR and CI are composed of a mixture of serpentine and saponite (Beck et al. 2010) while phyllosilicates found in IDPs are mainly saponites (Zolensky & Barrett 1994). Note that the band at 0.7 μm was not detected in the CI and CR spectra, but is present in the CM spectra, which

allows a comparison with asteroids showing signs of aqueous alteration (such as C-type). CM have therefore often been proposed as analogs to hydrated asteroids even if the correspondence is not perfect because meteorites have a center of band distributed between 0.71 and 0.75 μm slightly offset from the distribution observed on asteroids at 3σ: 0.65 and 0.74 μm (Burbine 1998; Fornasier et al. 2014). L2079C18 thus has a totally different aqueous alteration band position than that of CM meteorites and which, unlike meteorites, is located in the lower limit of the distribution of the asteroid band positions (see Figure 5(b)). This absorption band therefore makes this IDP a potential analog for hydrated asteroids, with major differences from CM-type analogs. Its band depth ($8.0 \pm 0.6\%$) does not perfectly match with that of the asteroids (up to 7% in the panel of Fornasier et al. 2014). This difference could be explained by other secondary processes such as space weathering, which generally reduce the intensity of the Vis–NIR spectral characteristics without changing their position too much (e.g., Marchi et al. 2005 and references therein), or by a grain size effect. The observation phase angle also influences the band depth, although a combination of these three processes is also possible. This particle is one of the few extraterrestrial materials with a strong phyllosilicate absorption band in the saponite region and in the lower limit of the distribution of the position band of hydrated asteroids. It could therefore be related to the surface of hydrated asteroids present in the main belt.

4.5. Magnetite Effect

Among the IDPs with sizes larger than the critical size (above 17 μm in equivalent diameter) for the wavelength range [0.45–1.0] μm, some particles (particles 1, 4, 5, 6, and 8) have a more or less marked higher-frequency reflectance decrease in the NIR range (Figure 3(a)). This falloff in reflectance may be due to the presence of silicate, silicate glasses, or to the presence of magnetite which is commonly found in chondritic IDPs (e.g., Christoffersen & Buseck 1986), it can be produced by different processes, such as the aqueous alteration of silicates on the parent body (e.g., McCollom 2016) and/or during the atmospheric entry (e.g., Germani et al. 1990; Toppani & Libourel 2003). The atmospheric entry inducing the heating of IDPs depends on their size, density, initial velocity, and entry angle (Love & Brownlee 1991). This induces various alteration processes, such as the formation of magnetite on their surface, the loss of volatiles as well as the transformation of phyllosilicates to anhydrous silicates with extreme heating of the IDPs (olivine and/or pyroxene; Sandford & Bradley 1989).

Magnetite is also commonly found in some meteorites that have undergone aqueous alteration such as CM, CR, and CI chondrites (e.g., Brearley & Jones 1998). Magnetite has also been suggested to be present on the surface of some types of asteroids (e.g., Yang & Jewitt 2010). Its presence has recently been suggested for Ryugu (C-type) (Le Corre et al. 2018) and Bennu (B-type; Lauretta et al. 2017; Hamilton et al. 2019).

In the Vis–NIR range (0.45–1.0 μm), magnetite has a typical spectrum that exhibits a minimum of the reflectance around 0.55 and 1.0 μm and the maximum of the reflectance in this range is around 0.65 μm. It also causes bluing in the 0.7–1.0 μm range of hydrated meteorite (CM) spectra (Izawa et al. 2019). However, the effect of magnetite is more subtle in the short wavelength region, indeed they showed that for chondritic materials with carbonaceous macromolecules at their surface, the 0.4–0.65 μm region is little affected by the presence of magnetite even in large quantities, the absorption being dominated by organic matter inducing thus an important reddening in this wavelength range. Magnetite in the presence of organic molecules will have no effect at short wavelengths (the spectrum will remain dominated by a reddening due to organic matter) but only in the range 0.7–1.0 μm, while in the absence of organic matter the range 0.4–0.65 μm can be affected by the presence of magnetite, causing a flattening or even a bluing of the spectrum in this range. Apart the L2079C18 (1), all other particles have a more or less red slopes in the short wavelengths (0.45–0.65 μm). Therefore, the co-existence of magnetite and organics on their surfaces can be hypothesized.

Magnetite could also have an effect on the reflectance level of particles. In fact, magnetite is a relatively dark material with reflectance level around 5%–8% (Izawa et al. 2019). Thus, a layer of magnetite formed on the surface of an initially shiny material (reflectance level >8%) will tend to darken this material. While on an initially very dark material (like IDPs), this could lead to an increase in the reflectance level up to a value close to that of magnetite if the layer of magnetite is large. The histogram in Figure 10 shows that the majority of IDPs have a level of reflectance compatible with that of magnetite. If we consider the reflectance level of all particles analyzed in this study except 15 (Figure 8) we observe that the particle 8 has a very high reflectance level ($\sim$12%) that could indicate that it is not affected by magnetite. Particles 4, 5, 6, 7_b, 9, 10, and 12 have low reflectance levels (<5%) that could may also indicate that they are not very affected by the presence of magnetite on the surface. While particles 1, 2, 3, 7_a and 11 have reflectance levels close to that of the magnetite that could indicate the presence of this one on their surfaces.

Far IR, Raman analyzes should confirm the presence or absence of magnetite in these particles. These measurements are planed for a forthcoming study.

5. Conclusion

Our Vis–NIR measurements performed on 15 IDPs of different sizes showed that

1. It is crucial to perform 20 rotations of 18° each and average the different spectra to obtain the reflectance spectrum of an isolated IDP.
2. For particles with size below $\sim$17 μm the slope increases linearly with decreasing particle sizes (Figure 6). This behavior is due to a bias encountered in the reflectance measurement in this size range, thus inducing a loss of the chemical information.
3. For particle sizes larger than $\sim$17 μm, the spectral slopes seem randomly distributed between ~ -0.3 and 0.4 μm^{-1}, and the spectra must therefore carry chemical information of the particle.
4. The reflectance levels of the studied IDPs are distributed in several groups: one of them has a very high level of reflectance ($\sim$12%). Other particles are distributed into two groups: a reflectance level <5% and a reflectance level close to 7% (Figure 8). This bimodality could indicate different chemical information between the two groups. As discussed in Section 4.5 the particles with reflectance levels $\leqslant$5% are probably free of magnetite on their surfaces or at least less altered than the particles

having their reflectance levels $\geqslant$7%. The reflectance level could thus be an indicator of the presence/absence of magnetite.

5. The IDP L2079C18 shows a strong absorption band at $\sim$0.66 μm (depth of 8.0 $\pm$ 0.6%) indicating the presence of phyllosilicates. We attributed this band to saponite, a common phyllosilicates type found in IDPs. Our work led us, for the first time, to the detection of a hydration feature in the Vis–NIR reflectance spectrum of an IDP.
6. The band position observed here ($\sim$0.66 μm) is in a good agreement with the band position of hydrated asteroids between 0.65 and 0.72 μm. Thus, this IDP could be a good analog of certain hydrated asteroids, differently from CM-type meteorites that have a hydration band between 0.71 and 0.75 μm. Our result reopens thus the debate about the origin of hydrated IDPs for which there is no clear consensus today.

Finally, the mineralogy of the studied IDPs will be investigated in a forthcoming work to find a link between the reflectance spectra and the composition of the studied particles.

We are grateful to the CAPTEM NASA for providing the IDPs. This work is supported by the Programme National de Planétologie (PNP) of CNRS/INSU, co-funded by CNES. The authors also thank the ANR RAHIIA_SSOM and the P2IO LabEx (ANR-10-LABX-0038) in the framework Investissements d'Avenir (ANR11-IDEX-0003-01) for their supports. We thank O. Mivumbi and Y. Longval for their help and technical support for the developement of the device.

References

Beck, P., Pommerol, A., Thomas, N., et al. 2012, Icar, 218, 364
Beck, P., Quirico, E., Montes-Hernandez, G., et al. 2010, GeCoA, 74, 4881
Bonal, L., Brunetto, R., Beck, P., et al. 2015, M&PS, 50, 1562
Bonal, L., Quirico, E., Bourot-Denise, M., et al. 2006, GeCoA, 70, 1849
Bradley, J. 1994, AIP Conf. Proc. 310, Analysis of Interplanetary Dust Particles (Melville, NY: AIP), 89
Bradley, J. P. 2003, in Treatise on Geochemistry, Vol. 1, ed. H. D. Holland & K K. Turekian (Amsterdam: Elsevier), 689
Bradley, J. P., Keller, L. P., Brownlee, D. E., et al. 1996, M&PS, 31, 394
Brearley, A. J. 1993, GeCoA, 57, 1521
Brearley, A. J., & Jones, R. H. 1998, in Planetary Materials, ed. J. J. Papike (Berlin: De Gruyter), 125
Brownlee, D. 1994, AIP Conf. Proc. 310, Analysis of Interplanetary Dust Particles (Melville, NY: AIP), 5
Brownlee, D. E., Joswiak, D. J., Schlutter, D. J., et al. 1995, LPSC, 26, 183
Brunetto, R., Borg, J., Dartois, E., et al. 2011, Icar, 212, 896
Burbine, T. H. 1998, M&PS, 33, 253
Burbine, T. H., & Binzel, R. P. 2002, Icar, 159, 468
Burbine, T. H., Buchanan, P. C., Binzel, R. P., et al. 2001, M&PS, 36, 761
Burbine, T. H., McCoy, T. J., Jaresowich, E., et al. 2003, AMR, 16, 185
Burns, R. G. 1993, Mineralogical Applications of Crystal Field Theory (Cambridge: Cambridge Univ. Press)
Bus, S. J., & Binzel, R. P. 2002, Icar, 158, 146
Campins, H., & Ryan, E. V. 1989, ApJ, 341, 1059
Christoffersen, R., & Buseck, P. R. 1986, E&PSL, 78, 53
Clark, B. E., Binzel, R. P., Howell, E. S., et al. 2011, Icar, 216, 462
Cloutis, E. A., & Gaffey, M. J. 1991, JGR, 96, 809
Cloutis, E. A., Gaffey, M. J., Jackowski, T. L., et al. 1986, JGR, 91, 641
Cloutis, E. A., Izawa, M. R. M., & Beck, P. 2018, in Primitive Meteoritesand Asteroids, ed. N. Abreu (Amsterdam: Elsevier), 273
Craig, M. A., Cloutis, E. A., & Bailey, D. T. 2007, LPSC, 38, 1356
DeMeo, F. E., Binzel, R. P., Slivan, S. M., et al. 2009, Icar, 202, 160
Dermott, S. F., Grogan, K., Gustafson, B. A. S., et al. 1996, in IAU Coll. 150, Physics, Chemistry, and Dynamics of Interplanetary Dust, ed. B. A. S. Gustafson & M. S. Hanner (San Francisco, CA: ASP), 143
Dermott, S. F., Nicholson, P. D., Burns, J. A., et al. 1984, Natur, 312, 505
Duke, M. B., & Silver, L. T. 1967, GeCoA, 31, 1637
Fornasier, S., Lantz, C., Barucci, M. A., et al. 2014, Icar, 233, 163
Gaffey, M. J. 1976, JGR, 81, 905
Gaffey, M. J., Bell, J. F., Brown, R. H., et al. 1993, Icar, 106, 573
Germani, M. S., Bradley, J. P., & Brownlee, D. E. 1990, E&PSL, 101, 162
Hahn, J. M., Zook, H. A., Cooper, B., et al. 2002, Icar, 158, 360
Hamilton, V. E., Simon, A. A., Christensen, P. R., et al. 2019, NatAs, 3, 332
Hapke, B. 2008, Icar, 195, 918
Hartman, B., & Domingue, D. 1998, Icar, 131, 421
Hergenrother, C. W., Maleszewski, C. K., Nolan, M. C., et al. 2019, NatCo, 10, 1291
Ipatov, S. I., Kutyrev, A. S., Madsen, G. J., et al. 2008, Icar, 194, 769
Izawa, M. R. M., Cloutis, E. A., Rhind, T., et al. 2019, Icar, 319, 525
Jewitt, D. 2012, AJ, 143, 66
Keller, L. P., & Buseck, P. R. 1990, GeCoA, 54, 2113
Kirkwood, D. 1891, Sidereal Messenger, 10, 194
Langevin, Y., Merouane, S., Hilchenbach, M., et al. 2020, P&SS, 182, 104815
Lauretta, D. S., Balram-Knutson, S. S., Beshore, E., et al. 2017, SSRv, 212, 925
Lauretta, D. S., Hergenrother, C. W., Chesley, S. R., et al. 2019, Sci, 366, 3544
Le Corre, L., Sanchez, J. A., Reddy, V., et al. 2018, MNRAS, 475, 614
Liou, J. C., Dermott, S. F., & Xu, Y. L. 1995, P&SS, 43, 717
Love, S. G., & Brownlee, D. E. 1991, Icar, 89, 26
Love, S. G., & Brownlee, D. E. 1993, Sci, 262, 550
Marchi, S., Brunetto, R., Magrin, S., et al. 2005, A&A, 443, 769
McCollom, T. M. 2016, PNAS, 113, 13965
McCord, T. B., Adams, J. B., & Johnson, T. V. 1970, Sci, 168, 1445
Merouane, S., Djouadi, Z., & Le Sergeant d'Hendecourt, L. 2014, ApJ, 780, 174
Messenger, S., Nakamura-Messenger, K., Keller, L. P., et al. 2015, M&PS, 50, 1468
Mustard, J. F., & Hays, J. E. 1997, Icar, 125, 145
Nesvorný, D., Bottke, W. F., Levison, H. F., et al. 2003, ApJ, 591, 486
Nesvorný, D., Jenniskens, P., Levison, H. F., et al. 2010, ApJ, 713, 816
Rietmeijer, F. 1998, in Planetary Materials, ed. J. J. Papike (Berlin: De Gruyter), 29
Rietmeijer, F. 2002, ChEG, 62, 1
Rubin, A. E. 1989, Metic, 24, 179
Sandford, S. A. 1987, FCPh, 12, 1
Sandford, S. A., & Bradley, J. P. 1989, Icar, 82, 146
Sandford, S. A., & Walker, R. M. 1985, ApJ, 291, 838
Schulz, R., Hilchenbach, M., Langevin, Y., et al. 2015, Natur, 518, 216
Sears, D. W. G., & Dodd, R. T. 1988, Meteorites and the Early Solar System (Tucson, AZ: Univ. Arizona Press), 3
Sugita, S., Honda, R., Morota, T., et al. 2019, Sci, 364, 252
Sunshine, J. M., Binzel, R. P., Burbine, T. H., et al. 1997, AAS DPS Meeting 29, 29, 05.03
Tholen, D. J., & Barucci, M. A. 1989, Asteroids II (Tucson, AZ: Univ. Arizona Press), 298
Thomas, K. L., Blanford, G. E., Clemett, S. J., et al. 1995, GeCoA, 59, 2797
Tomeoka, K., & Buseck, P. R. 1990, GeCoA, 54, 1745
Toppani, A., & Libourel, G. 2003, GeCoA, 67, 4621
Tsumura, K., Battle, J., Bock, J., et al. 2010, ApJ, 719, 394
Urey, H. C., & Craig, H. 1953, GeCoA, 4, 36
Vernazza, P., Marsset, M., Beck, P., et al. 2015, ApJ, 806, 204
Verpoorter, C., Carrère, V., & Combe, J.-P. 2014, JGRF, 119, 2098
Watanabe, S., Hirabayashi, M., Hirata, N., et al. 2019, Sci, 364, 268
Wooden, D. H. 2002, EM&P, 89, 247
Wooden, D. H. 2008, SSRv, 138, 75
Yang, B., & Jewitt, D. 2010, AJ, 140, 692
Yang, H., & Ishiguro, M. 2015, ApJ, 813, 87
Zolensky, M. E., & Barrett, R. A. 1994, Metic, 29, 616